Aramid Nanofibers Reinforced Cellulose Paper-Based Lithium-Ion Battery Separator with Improved Safety and Cycling Stability

Sufeng Zhang (sufengzhang@126.com)
Shaanxi University of Science and Technology https://orcid.org/0000-0001-7109-0355
Jin Luo
Shaanxi University of Science and Technology Xi\'an Campus: Shaanxi University of Science and Technology
Min Du
Shaanxi University of Science and Technology Xi'an Campus: Shaanxi University of Science and Technology
Hongying Hui
Shaanxi University of Science and Technology Xi\'an Campus: Shaanxi University of Science and Technology

Research Article

Keywords: Lithium-ion batteries, Cellulose-based separator, Aramid nanofibers, High safety, Stable cycling performance

Posted Date: August 10th, 2021

DOI: https://doi.org/10.21203/rs.3.rs-755828/v1

Abstract

Commercial polyolefin separators with poor electrolyte wettability and inferior thermal stability have hampered the development of advanced lithium-ion batteries (LIBs) due to their unsatisfied electrochemical performance and severe safety hazards. Herein, a novel paper-based composite separator composed of electrolyte-affinitive cellulose fibers (CFs) and thermally stable aramid nanofibers (ANFs) was successfully fabricated through the traditional papermaking method. It was found that the incorporation of ANFs played crucial roles in improving the defects of pure CF separator such as large-sized pores, low mechanical strength and high flammability. Specifically, the CF/ANF composite separator with 20 wt.% ANFs (CF/ANF-20) possessed narrow micropores, satisfied tensile strength (33MPa), excellent thermal resistance (without dimensional shrinkage up to 200 °C) and flame retardancy, greatly enhancing the safe operation of battery. In addition, benefiting from the highly porous structure and exceptional electrolyte affinity of CF separator, the CF/ANF-20 composite separator exhibited appropriate porosity and superior electrolyte wettability, which brought about a high electrolyte uptake (157%), thus endowing it with better ionic conductivity (0.75 mS cm^{-1}) and lower interfacial resistance than that of commercial polypropylene (PP) separator. Accordingly, the LiFePO4/Li half cells using CF/ANF-20 separator delivered outstanding rate capability and stable cycling performance. All results indicate that the CF/ANF-20 separator with great balance between the electrochemical performance and safety is an intriguing candidate for advanced LIBs.

Introduction

Nowadays, rechargeable lithium-ion batteries (LIBs) have been recognized as the most reliable energy storage devices for portable electronic products and electronic vehicles by reason of their high energy density, long lifetime and environmental friendliness (Costa et al. 2020; Manthiram 2017). As a key element of LIB, the separator provides a porous ion-transport channel while separating the cathode and anode to prevent internal short-circuits, thus directly affecting the cell performance and safety. (Jana et al. 2018; Zhai et al. 2021). Conventionally, the widely commercialized LIB separators are microporous polyolefin membranes comprised of polyethylene (PE) or polypropylene (PP) due to their uniform pore size, high mechanical strength and good electrochemical stability (Costa et al. 2019). However, these separators still encounter the drawbacks of low porosity and bad electrolyte wettability, which damage the electrolyte storage and the transport of Li^+, thus resulting in low ionic conductivity and inferior battery performance. In addition, the poor thermostability of polyolefin separators would cause internal short-circuits at elevated temperatures and eventually lead to the explosion of LIBs (Cha et al. 2018; Waqas et al. 2019). Therefore, considerable efforts have been made to develop advanced separators that can satisfy the increasing demand of high-performance LIBs (Zhang et al. 2021a).

Cellulose paper-based separators, as one of the promising alternatives of polyolefin separators, have so far garnered considerable attention owing to their intriguing properties, such as high porosity, good electrolyte wettability and excellent chemical resistance (Jabbour et al. 2013; Sheng et al. 2017). Furthermore, cellulose materials combining the features of natural abundance, sustainability and low

cost are more attractive for separator application in contrast to the petroleum-based polyolefin materials due to the exhausted fossil fuel and severe environmental problems (Zhang et al. 2020). However, normal cellulose paper is inappropriate for direct use as the LIB separator due to its relatively large-sized pores and poor mechanical strength, which can bring about serious self-discharge and other safety risks caused by the formation of lithium dendrites (Zhang et al. 2019). With the aim to address these problems, numerous endeavors have been exerted. For example, some inorganic ceramic particles such as Al_2O_3 and SiO_2 have been adopted as the coating layer or additives to minimize the large pores of cellulose paper separator (Wang et al. 2018; Xu et al. 2017). Unfortunately, restricted by the poor adhesion of ceramic particles which are readily detached from the paper substrate, these paper-supported inorganic composite separators were not beneficial for the long-term practical operation of LIBs. Recently, Lv et.al fabricated a composite cellulose paper (CCP) separator combined with cellulose nanofibrils (CNFs) through the filtration process (Lv et al. 2021). The favorable length to width ratio and nanoscale of CNFs was used to fill the large pores created by the networks of cellulose fibers (CFs). It was found that the CCP separator showed narrow pore size distribution, superior electrolyte wettability and enhanced mechanical strength, yielding good working stability for the $LiCoO_2$/Li batteries. Disappointingly, the pure cellulose paper separator is highly flammable, which is unfavorable for mitigating safety concerns when LIBs suffer from thermal runaway under harsh conditions (Zhang et al. 2021b). In this case, the scientific community has paid much attention to the development of flame-retardant cellulose paper separators. Incorporating flame retardants into cellulose pulps during the homogeneous mixing process has been considered an efficient method to enhance the flame retardance of cellulose paper separators (Zhang et al. 2014). Moreover, the flammability of cellulose paper separators can be improved by compounding cellulose fibers with suitable fire-resistant materials, such as hydroxyapatite nanowires, xonotlite nanowires and calcium alginate (Jia et al. 2020; Li et al. 2017; Tan et al. 2020). However, these modification strategies provide limited improvement in the mechanical properties of cellulose paper separators. Therefore, the pursuit of high-performance cellulose paper separators with appropriate pore size, superb mechanical strength and enhanced flame retardance remains an ongoing challenge.

As a novel one-dimensional nanomaterial, aramid nanofibers (ANFs) possess exceptional mechanical properties and thermal resistance, allowing them to be promising material for the design of high-performance battery separators (Yang et al. 2020a). For instance, Hu et al. fabricated an ANF-modified PP separator through the simple dip-coating method (Hu et al. 2016). The modified PP separator presented comparable mechanical strength as well as increased thermal stability and C-rate performance in comparison with the pristine PP separator. Zhu et al. reported an ANFs/polyphenylene sulfide composite separator, which exhibited good tensile strength and self-extinguishing characteristic (Zhu et al. 2019). Meanwhile, ANF paper was also developed as LIB separator, which had substantial advantages in the electrolyte wettability, mechanical property and flame retardance compared to the commercial polyolefin separators (Patel et al. 2020). Nevertheless, these separators still rely on the consumption of large amounts of petroleum-based materials, which inevitably gives rise to environmental concerns and relatively high costs. Thus, this makes us to envision the possibility of introducing ANFs into the sustainable and cost-effective cellulose paper separator.

Herein, inspired by the advantages of cellulose and ANFs in LIB separator applications, a novel paper-based composite separator (CF/ANF) composed of cellulose fibers and aramid nanofibers was fabricated through the facile papermaking method. Given that highly porous and electrolyte-affinitive cellulose paper benefits the absorption of liquid electrolyte and promotes the migration of Li^+, cellulose fibers were deliberately selected for the construction of separator backbone. Besides, based on the high aspect ratio and polar aramid component, the introduced aramid nanofibers were expected to optimize the relatively large pores and insufficient mechanical and thermal properties of pure cellulose paper separator. The porous structure, mechanical strength, thermal stability, electrolyte wettability and electrochemical performance of the as-prepared CF/ANF separator were systematically evaluated. It was demonstrated that the CF/ANF composite paper with high safety and excellent electrochemical performance could be a promising alternative for advanced LIB separators.

Experimental

Materials

Poly(para-phenylene terephthamide) (PPTA) fibers were obtained from the Dupont Group. Cellulose paper (NKK TF40) composed of solvent-spun regenerated cellulose fibers was purchased from Nippon Kodoshi Corporation (Japan). Commercial PP separator (Celgard 2400) was provided by Celgard Company (USA). Liquid electrolyte consisting of 1 M lithium hexafluorophosphate ($LiPF_6$) in ethylene carbonate (EC)/dimethyl carbonate (DMC)/ethyl methyl carbonate (EMC) (1/1/1, v/v/v) was purchased from Nanjing Mojiesi Energy Technology Co., Ltd. Lithium (Li) metal, lithium iron phosphate ($LiFePO_4$) sheet and battery case (LIR 2032) were provided by Shenzhen Kejing Star Technology Co., Ltd, China (battery grade). All other chemical reagents like dimethyl sulfoxide (DMSO), potassium hydroxide (KOH) and ethanol were obtained commercially and used without any further purification.

Preparation of ANFs suspension

A stable ANFs suspension was obtained from the deprotonation and dissociation of PPTA fibers according to Yang's method (Yang et al. 2011). Briefly, 0.3 g KOH was firstly dissolved in 4 ml deionized water to obtain the uniform KOH solution. Then, 0.2 g PPTA fibers, 100 ml DMSO and the resultant KOH solution were mixed and magnetically stirred for about 4h at room temperature to form the homogeneous dark red solution of ANFs/DMSO. Afterwards, 200 ml deionized water was injected into the solution under vigorous stirring, making the flocculent ANFs fully precipitated. The following purification and separation of ANFs were achieved by repeatedly washing the colloidal ANFs with alcohol and deionized water through vacuum assisted filtration. Finally, the purified ANFs were diluted with deionized water to reach a homogeneous ANFs/H_2O suspension (0.5 mg/mL).

Preparation of the CF/ANF paper-based composite membranes

The schematic illustration for the preparation of CF/ANF composite membranes was shown in Fig. 1. Firstly, cellulose paper was smashed by a PFI beater for 10000 revolutions to yield the fibrillated cellulose fibers pulp. Next, the obtained cellulose fibers pulp was fully dispersed in deionized water at a concentration of 0.5 mg/mL with vigorous magnetic stirring. Then, at a fixed basis weight of 25 g/m^2, cellulose fibers and ANFs suspensions were mixed with the proportion of 9:1, 8:2 and 7:3 (w/w), respectively, and subsequently filtrated under vacuum to fabricate a series of wet composite membranes. Finally, all the wet membrane samples were pressed in a paper presser at 0.4 MPa for 5 min and then dried under vacuum at 105°C for 10 min. The prepared CF/ANF composite membranes were correspondingly denoted by CF/ANF-10, CF/ANF-20 and CF/ANF-30, according to the percent of ANFs contents. Meanwhile, pure cellulose membrane without the introduction of ANFs was also prepared at the same procedure and named as CF.

Characterization

The microstructure of ANFs in water was investigated by transmission electron microscopy (TEM, FEI Tecnai G2 F20 S-TWIN, USA). The surface morphologies of the membranes were observed via scanning electron microscope (SEM, HITACHI-S4800, Japan) at an accelerating voltage of 5.0 kV. Fourier transform infrared spectroscopy (FTIR) spectrometer (VECTOR22, Bruker, German) was used to determine the chemical components of the membranes. The pore size distribution of the membranes was measured by using automatic mercury porosimeter. The porosity (P) of the membranes was determined by immersing them in n-butanol for 2 h and then calculated by the following Eq. (1):

$$P\ (\%) = (\Delta m/\rho_b)/V_s \times 100\% \quad (1)$$

where Δm is the weight deviation between the saturated and dry membrane, ρ_b and V_s are the density of n-butanol (0.81 g/mL) and the volume of dry membrane, respectively.

Likewise, the electrolyte uptake (EU) of the membranes was measured according to the following Eq. (2):

$$EU = (M_{wet} - M_{dry}) / M_{dry} \times 100\ \% \quad (2)$$

where M_{dry}, M_{wet} are the weight of the membranes before and after soaking in the liquid electrolyte for 2 h.

The mechanical properties of the membranes (30 mm × 10 mm) were tested by a universal tensile tester (AI-7000-NGD, Goodtechwill, China) at a drawing speed of 5 mm min^{-1}.

To evaluate electrolyte wettability of the membranes, electrolyte wetting behavior was observed by dripping electrolyte droplet (10 μL) on membrane surface. Optical contact angle measuring device (OCA20, Dataphysics, Germany) was used to record the static contact angles of water and electrolyte droplets (5 μL). The capillary absorption height was further tested by immersing one end of the membrane sample in electrolyte for 1 h.

Thermal properties of the membranes were investigated through thermogravimetric analyzer (STA449F3, NETZSCH, Germany) from 20 to 600 ℃ at 10 ℃/min under the nitrogen gas atmosphere and differential scanning calorimeter (STA449F3, NETZSCH, Germany) from 20 to 300 ℃ at 10 ℃/min under the nitrogen gas atmosphere. Thermal shrinkage behavior was measured by comparing the dimensional change of the membranes after heat treatment (25, 120, 160 and 200°C) in an oven for 0.5 h. Combustion test was carried out to evaluate the flame retardancy of the membranes.

Electrochemical Measurements

The ionic conductivity and interfacial resistance of the separators were evaluated through electrochemical impedance spectroscopy (EIS) measurements in a frequency region of 0.1 to 10^5 Hz. For the ionic conductivity test, a symmetrical SS/separator/SS cell was assembled by placing the electrolyte-soaked separator between two stainless steel (SS) electrodes. The ionic conductivity (σ, mS cm^{-1}) was calculated according to the following Eq. (3):

$$\sigma = d/(R_b \cdot S) \quad (3)$$

where d (cm), S (cm^{-2}) and R_b (Ω) are the thickness, efficient area and bulk resistance of separator sample, respectively.

Similarly, a symmetrical Li/separator/Li cell was assembled to assess the interfacial resistance between separator and Li electrode.

The electrochemical stability window of separators was evaluated by assembling the SS/separator/Li cell through linear sweep voltammetry (LSV) test with the potential range from 3.0 to 5.5 V (vs. Li^+/Li) under a scan rate of 5.0 mV s^{-1}.

These EIS and LVS measurements were fully conducted on an electrochemical workstation (CHI 760e, CH Instruments) at room temperature.

To evaluate the charge/discharge performance, half-cells (2032-type) were assembled by sandwiching the electrolyte-soaked separator (PP, CF and CF/ANF-20, respectively) between a $LiFePO_4$ cathode and a lithium foil anode. All the cells were assembled in an argon-filled glove box (Lab 2000, O_2 and H_2O < 0.1 ppm) and tested on a LAND battery instrument (CT3001A, Wuhan LAND Electronic., Co, Ltd, China) under a cut-off voltage range from 2.5 to 4.2 V.

The rate capability was investigated at different charge/discharge current densities varied from 0.2 to 3.0 C (0.2 C, 0.5 C, 1 C, 2 C and 3 C). Moreover, cycling performance was appraised at 25°C with a fixed charge/discharge current density of 0.5 C/0.5 C.

Results And Discussion

Morphology and structure

Figure 2 displayed the surface morphologies of ANFs and the membrane samples. It could be observed from Fig. 2(a) that the as-prepared ANFs were homogeneously distributed and the mean fiber diameter was approximately 36 nm (Fig. S1). As shown in Fig. 2(b), the commercial PP membrane presented a uniform and elliptic pore structure with an average pore size of about 77 nm (Fig. S2) due to the uniaxial stretching technology during the manufacturing process (Lee et al. 2014). By contrast, extremely large and irregular pores were seen in the CF membrane (Fig. 2c). This structure was beneficial to the fast transportation of Li^+ between the cathode and anode, yielding good rate performance for the battery. However, the large-sized pores of CF membrane easily caused self-discharge and internal short-circuits arising from lithium dendrite growth or the migration of electrode particles (Boateng et al. 2021; Pan et al. 2017). Thus, aramid nanofibers with different ratios were introduced to regulate the pore size of CF membrane through the facile filtration process. As illustrated in Figs. 2(d-f), the uniformly distributed ANFs connected and intertwined with the relatively loose cellulose fibers, constructing more nanosized pores for the CF/ANF membranes. The pore size distribution of these membranes examined here was depicted in Fig. 3(a). Apparently, the pore size values of CF membrane decreased significantly with the addition of ANFs. As ANFs ratio increased to 20 wt.%, the obtained CF/ANF-20 membrane displayed smaller pore size (average pore size around 410 nm) and narrower pore size distribution than that of CF and CF/ANF-10 membranes, making it more suitable for serving as the LIB separators.

The chemical composition of CF/ANF composite membranes was identified by FTIR spectroscopy in Fig. 3(b). It was seen that the pure ANF membrane showed several unique characteristic peaks around 3300 cm^{-1} (N-H stretching vibration), 1650 cm^{-1} (C = O stretching vibration in amide), 1540 cm^{-1} (N-H bending vibration) and 1510 cm^{-1} (C = C stretching vibration in aromatic ring) (Liu et al. 2020a). With regard to pure CF membrane, the broad absorption peak at 3200–3600 cm^{-1} corresponded to stretching vibration of O-H groups. The peak at 2891 cm^{-1} was assigned to the stretching vibration of C–H bonds. Besides, the strong absorption peak at 1010 cm^{-1} could be ascribed to the C–O stretching vibration in C-O-C or C-OH groups (Nabipour et al. 2019). Upon the addition of ANFs, the characteristic peaks of ANFs were clearly detected in all the composite membranes. Moreover, the intensity of these peaks tended to increase as the ANFs content increases. These results fully confirm that different ratios of ANFs have been successfully introduced into the CF membrane matrix.

It is well known that high porosity is required for LIB separators to store liquid electrolyte and provide more channels for the transfer of Li^+, thus enabling superior electrochemical properties (Sheng et al. 2020). The porosity and electrolyte uptake of the membranes were calculated and depicted in Fig. 3(c). The CF membrane showed the highest porosity (59.6%) and electrolyte uptake (223.6%), which were nearly 1.5 and 2.4 times higher than that of PP membrane, respectively. These characteristics were believed to originate from its interconnected and macroporous structure as seen in the SEM image. However, the addition of ANFs ratios from 10–30% had a negative impact on the porosity of CF membrane, which might be ascribed to the fact that excessive ANFs could fill or even block the pores of CF membrane, resulting in dense morphology and reduced porosity. Meanwhile, the electrolyte uptakes among the CF/ANF composite membranes were observed to decrease in a similar trend with the porosity.

Remarkably, the CF/ANF-30 membrane had a relatively low electrolyte uptake (96.5%) due to its lowest porosity (40.2%), which would increase the internal resistance of battery when acting as the separator (Huang et al. 2021).

Mechanical properties

LIB separators are supposed to possess high mechanical properties that can withstand the high tension from cell assembly and the growth of lithium dendrites formed during prolonged cycling (Mao et al. 2021). The tensile strength and modulus of the membranes were surveyed via the tensile test. As seen in Fig. 3(d), the CF membrane showed a weak tensile strength of 7 MPa due to the incompact connection of cellulose fibers. In contrast, the tensile strength of CF/ANF membranes significantly increased along with the addition of ANFs, and the CF/ANF-30 membrane possessed the highest tensile strength (48 MPa). Although PP membrane had a high tensile strength of 111 MPa along the machine direction (Fig. S3), its tensile strength at transverse direction was only recorded as 15 MPa, much lower than that of CF/ANF composite membranes due to the uniaxial stretching technology (Hao et al. 2020). Besides, the introduction of ANFs also showed a reinforcing effect on Young's modulus of CF membrane, which was more advantageous relative to PP membrane (Fig. S4). According to previous literatures, high Young's modulus was conducive to sustain mechanical integrity and avoid the rupture of separators when an unexpected collision happened (Liu et al. 2018; Zhu et al. 2020). The improved mechanical properties of CF/ANF membranes not only stemmed from the uniform dispersion of ANFs in CF membrane matrix, but also the effective interaction between ANFs and cellulose fibers through hydrogen bonds. It was worth noticing that the CF/ANF-20 membrane possessed superior tensile strength than most of other cellulose-based separators (Table S1), which would guarantee the safe operation of LIBs under rigorous conditions.

From a practical perspective, an ideal LIB separator should possess the critical parameters including small and uniform pore size, high porosity and electrolyte uptake, robust mechanical strength, good electrolyte wettability as well as excellent thermal stability to enable superior battery performance (Deimede and Elmasides 2015). As listed in Table 1, the obtained CF/ANF-20 membrane with tailored pore size, appropriate porosity and mechanical strength, which was more hopeful to achieve the trade-off between high safety and electrochemical performance of LIB, was thus chosen as the separator for further investigations.

Table 1
Physical properties of the PP, CF and CF/ANF composite membranes.

	Thickness /μm	Mean pore size /μm	Porosity /%	Electrolyte uptake/%	Tensile strength/MPa
PP	25	0.077	41.0	92.3	15
CF	45	1.76	59.6	223.6	7
CF/ANF-10	42	0.90	54.3	185.1	21
CF/ANF-20	40	0.41	49.5	157.4	34
CF/ANF-30	37	0.32	40.2	96.5	48

Electrolyte wettability and thermal stability

Good electrolyte wettability is in critical need for LIB separator to accelerate the battery assembly process and promote efficient Li^+ transport between the electrodes (Huang et al. 2019). As shown in Fig. 4(a), after dropping equal volume of liquid electrolyte on each separator surface, the electrolyte droplet did not well diffuse on PP separator for a long time, while the entire CF and CF/ANF-20 separators were rapidly wetted within 30 s. The contact angles of water and liquid electrolyte (LE) were also measured and displayed in Fig. 4(b). It was clearly found that the water contact angle of PP separator was up to 104.6° due to the lyophobic nature of PP. Likewise, a high LE contact angle of 43.9° was recorded for PP separator, indicating its poor electrolyte wettability. In contrast, the CF separator contained numerous polar groups (hydroxyl groups), endowing it with the smallest water and LE contact angles. A slight increase of contact angles was observed for the CF/ANF-20 separator, which mainly resulted from the decrease of free hydrophilic groups in cellulose and ANFs due to the formation of abundant hydrogen bonds (Luo et al. 2019). Furthermore, the electrolyte wettability of various separators was quantitatively evaluated through the electrolyte immersion-height measurements. As seen from Fig. 4(c), when soaking in the liquid electrolyte for 1 h, the final immersion heights of CF and CF/ANF-20 separator samples were about 12 mm and 7 mm, respectively, which were both much higher than that of PP separator (3 mm). The above results explicitly demonstrated the excellent electrolyte wettability of CF-based separators, which was attributed to their highly porous structure as well as the strong affinity of cellulose and ANFs with the polar electrolyte mixture (Fig. 4(d)).

High thermal stability is another pivotal parameter for LIB separator, which can ensure the safety and lifetime of battery since local heating may take place under rigorous conditions (e.g., battery overheating, overcharging, and overcurrent) (Feng et al. 2020; Wen et al. 2019). The TG and DSC measurements were carried out to evaluate the thermal stability of the separators. As shown in Fig. 5(a), the weight of PP separator sharply dropped at approximately 350°C due to the degradation of polyolefin backbone, and a

weight loss of 100% was reached for the PP separator when the temperature elevated to 500°C (Tan et al. 2020). For the CF separator, two distinct stages of weight loss were observed. The first stage was a slight weight loss of water moisture (before 200°C). The second stage from 250 to 350°C was a major weight loss, arising from the degradation of cellulose backbone (Chen et al. 2020). Additionally, one minor weight loss occurred at about 520°C for the CF/ANF-20 composite separator, corresponding to the degradation of ANFs polymer backbone (Luo et al. 2019). Meanwhile, the remaining weight of CF and CF/ANF-20 separators was respectively determined to be 13.8 and 30.5 wt. % at 500°C, indicating that the addition of ANFs could help to enhance the thermal stability of CF separator. Furthermore, it was observed from DSC curves (Fig. 5(b)) that the endothermic peak of PP separator appeared at about 165°C, which could be assigned to the melting of PP and caused the shutdown of micropores (Xu et al. 2019). In contrast, no obvious endothermic peak was recorded below 300°C for the CF-based separators, demonstrating the high stability in the pore structure of CF-based separators at high temperatures.

Since the shape change of separators will cause the physical contact between cathode and anode, thus leading to internal short-circuits of battery. Therefore, the dimensional thermal stability of different separators was also investigated through the thermal shrinkage tests. As shown in Fig. 5(c), the dimension of PP separator was inclined to decrease with the elevation of temperature. Particularly, the PP separator suffered from great shrinkage after heat treatment at 160°C for 0.5 h, and its thermal shrinkage rate reached almost 100% at 200°C. In sharp contrast, no apparent dimensional change was observed for the CF and CF/ANF-20 separators when the heating temperature approached 200°C. This behavior was attributed to the strong skeleton provided by cellulose fibers and outstanding thermal resistance of ANFs, which enabled the CF-based separators to resist thermal shrinkage substantially (Yang et al. 2020b). Nonflammability is also a critical necessity for high-performance LIB separators because it can prevent the battery from catching fire or exploding when thermal runaway happens (Zhang et al. 2021b). It could be found from Fig. 5(d) that the PP and CF separators were rapidly ignited and burnt out as soon as exposed to a flame. This phenomenon was consistent with previous literatures (Jia et al. 2020; Zhang et al. 2014). However, the CF/ANF-20 separator exhibited excellent self-extinguishing ability and even remained intact as a result of the high thermal stability of polyaramid nature (Liu et al. 2021; Patel et al. 2020). These results indicate that the CF/ANF-20 separator with superior thermal stability and flame-retardant capability is a promising candidate for highly safe LIBs.

Electrochemical performance of the separators

The ionic conductivity and interfacial resistance are regarded as two key factors of separator that greatly affects the performance of LIBs (Arora and Zhang 2004). Figure 6(a) showed the Nyquist plots measured by EIS at room temperature, where the intercept of the real axis corresponded to the bulk resistance (R_b) of separators. It was observed that the R_b were 3.40 Ω, 1.15 Ω, 2.30 Ω, 2.72 Ω and 5.72 Ω for the PP, CF, CF/ANF-10, CF/ANF-20 and CF/ANF-30 membranes, respectively. Then based on Eq. (3), the ionic conductivity of the membranes was calculated to be 0.38 mS cm^{-1}, 2 mS cm^{-1}, 0.93 mS cm^{-1}, 0.75 mS cm^{-1} and 0.33 mS cm^{-1}, respectively (Fig. 6(b)). The interconnected porous structure, excellent electrolyte wettability and uptake, which could boost the transport of Li^+ between electrodes, should be

responsible for the superior ionic conductivity of CF membrane. However, the ionic conductivity of CF/ANF composite membranes decreased with the increase of ANFs content, which might be explained from the aforementioned blocking function of ANFs in composite membranes. In particular, the ionic conductivity of CF/ANF-30 membrane was inferior to that of PP membrane due to its dense structure, which greatly limited its application in high-performance LIBs. Additionally, the interfacial resistance between the separator and Li electrode was also investigated by assembling Li-symmetrical batteries. Figure 6(c) showed the corresponding Nyquist plots of different separators, where the semicircle diameter in the middle frequency represented the interfacial resistance. It was obviously found that the interfacial resistance of PP, CF and CF/ANF-20 separator was approximately 310 Ω, 250 Ω and 280 Ω, respectively. The better interfacial compatibility of CF-based separators was mainly attributed to their excellent electrolyte wettability and absorption behavior, which improved the interfacial contact with Li electrode, thus facilitating Li^+ diffusion at the separator/electrode interface (Liu et al. 2020b).

The linear sweep voltammetry (LSV) tests were carried out to evaluate the electrochemical stability window of separators, which was crucial for determining the operation voltage of LIBs. As seen in Fig. 6(d), no obvious oxidation decomposition potential was observed up to 5.5 V vs Li/Li^+ for the CF separator, while the electrolyte-soaked CF/ANF-20 separator began to decompose at approximately 4.8 V vs Li/Li^+, indicating that the introduction of ANFs resulted in inferior electrochemical stability due to the Lewis base aramid component (Yang et al. 2020b). However, the electrochemical stability window of CF/ANF-20 separator was still broader than that of PP separator (4.3 V vs Li/Li^+) due to its superior affinity with carbonate electrolyte. These results suggest that the CF-based separators with high electrochemical stability are qualified for applications in high-voltage LIBs (Wen et al. 2017).

Battery performance

Battery performance was further tested in a $LiFePO_4$/separator/Li system, which could effectively evaluate the long-term stability of separators in LIBs (Liu et al. 2020b). The discharge rate capability of batteries with different separators was firstly investigated at various current densities ranging from 0.2 C to 3 C. Fig. S5 displayed the initial charge/discharge curves of $LiFePO_4$/Li batteries assembled with CF, CF/ANF-20 and PP separators at 0.2 C. It could be found that the batteries with CF and CF/ANF-20 separators delivered higher discharge capacities of 162.9 mA h g^{-1} and 159.4 mA h g^{-1}, respectively, which were 95.8% and 93.8% of the theoretical capacity of $LiFePO_4$ (170 mA h g^{-1}). In contrast, the initial discharge capacity of battery containing PP separator was only 153.2 mA h g^{-1}. Moreover, a downward trend was observed for the discharge capacity of all batteries with the increase of discharge current density as shown in Fig. 7(a). Particularly, the corresponding discharge capacities of batteries based on CF, CF/ANF-20 and PP separators decreased to 109.9 mA h g^{-1}, 98.7 mA h g^{-1} and 83.4 mA h g-1 at a high rate of 3 C. This phenomenon revealed the capacity loss caused by the increased ohmic polarization effect and serious over potential (i.e., IR drop) at high current density (Yang et al. 2021). Notably, the battery with CF separator showed the highest discharge capacity at all C-rates. This might be ascribed to the superior ionic conductivity and lowest interfacial resistance of CF separator, which could slow down

ohmic polarization degree in LIBs (Fig. S6) (Zhu et al. 2020). Furthermore, the capacity divergency between the cells with CF/ANF-20 separator and PP separator became more striking as the discharge rate increased, suggesting better rate capability of CF/ANF-20 separator than that of PP separator (Fig. 7(b)). More attractively, when the discharge current returned to 0.2 C, the discharge capacity of batteries could recover to their initial values, implying the good reversibility of cells using these separators.

The cycling performance of batteries with three separators were tested at a constant charge/discharge current density of 0.5C/0.5C at 25°C. As shown in Fig. 7(c), although the battery with CF separator initially displayed a high discharge capacity of 149.8 mA h g^{-1}, its final discharge capacity was only maintained at approximately 92.1 mA h g^{-1} after 100 cycles, indicative of a capacity retention of 61.5%. As a comparison, the discharge capacity retention of the battery with CF/ANF-20 separator was about 89.6% (decreased from 145.4 mA h g^{-1} to 130.3 mA h g^{-1}), which was also higher than that of PP separator (82.8%). Additionally, the coulombic efficiency was found to be nearly 100% for the battery using CF/ANF-20 separator during 100 cycles, but was relatively low at first cycle due to the generation of solid electrolyte interfacial (SEI) layer (Xu et al. 2019). The severe capacity degradation and poor cycling performance of CF-based battery mainly arose from the non-homogeneous pores of the CF separator, through which a mass of lithium dendrites could be formed as a consequence of the undistributed deposition of Li^+, therefore leading to the depletion of liquid electrolyte and formation of thick SEI layer (Lv et al. 2021; Zhang et al. 2015). Moreover, the thick SEI layer increased the interfacial resistance of battery (Fig. 7(d)), which further caused severe polarization effect and deteriorated the cycling stability of battery (Fig. S7). Fortunately, with the optimized pore size, high electrolyte adsorption and superior mechanical strength, the CF/ANF-20 separator was able to provide rapid and uniform ionic transport, as well as suppress the growth of lithium dendrites, thus endowing the battery with better cycling performance during long-term running (Du et al. 2019; Tan et al. 2020).

Conclusions

In this study, a novel ANFs reinforced cellulose paper with controllable pore structure, superior electrolyte wettability and high thermal stability was successfully developed as an advanced LIB separator. It could be found that the obtained CF/ANF-20 composite separator (with ANFs content of 20%) alleviated the risks of pure cellulose separator including large pore sizes, poor mechanical strength and high flammability which severely threaten the safety of LIBs. In comparison with the commercial PP separator, the CF/ANF-20 separator exhibited higher electrolyte uptake and superior electrolyte wettability, thus giving preferable ionic conductivity (0.75 mS cm^{-1}), lower interface resistance and better electrochemical stability. Meanwhile, the CF/ANF-20 separator could effectively prevent thermal runaway due to its excellent thermal resistance (without dimensional shrinkage up to 200°C) and flame retardancy. These advantages were ultimately confirmed to endow the $LiFePO_4$/Li half cells using CF/ANF-20 separator with outstanding rate capability and good cycling performance (discharge capacity retention up to 89.6% after 100 cycles). All results convincingly prove that the CF/ANF-20 separator present great potential application in high-performance and safe LIBs.

Declarations

Acknowledgments

This work was supported by the National Natural Science Foundation of China (Grant No.22078187) and the International Joint Research Center for Biomass Chemistry and Materials, the Shaanxi International Science and Technology Cooperation Base (2018GHJD-19). We thank LetPub (www.letpub.com) for its linguistic assistance during the preparation of this manuscript.

Conflicts of Interest: The authors declare no conflict of interest.

References

1. Arora P, Zhang ZM (2004) Battery Separators Chemical Reviews 104:4419–4462 doi:10.1021/cr020738u
2. Boateng B et al. (2021) Recent advances in separator engineering for effective dendrite suppression of Li-metal anodes Nano Select 2:993-1010 doi:10.1002/nano.202000004
3. Cha H, Kim J, Lee Y, Cho J, Park M (2018) Issues and Challenges Facing Flexible Lithium-Ion Batteries for Practical Application Small 14:1702989 doi:10.1002/smll.201702989
4. Chen Q, Zuo X, Liang H, Zhu T, Zhong Y, Liu J, Nan J (2020) A Heat-Resistant Poly(oxyphenylene benzimidazole)/Ethyl Cellulose Blended Polymer Membrane for Highly Safe Lithium-Ion Batteries ACS applied materials & interfaces 12:637-645 doi:10.1021/acsami.9b17374
5. Costa CM, Lee YH, Kim JH, Lee SY, Lanceros-Méndez S (2019) Recent advances on separator membranes for lithium-ion battery applications: From porous membranes to solid electrolytes Energy Storage Materials 22:346-375 doi:10.1016/j.ensm.2019.07.024
6. Costa CM, Lizundia E, Lanceros-Méndez S (2020) Polymers for advanced lithium-ion batteries: State of the art and future needs on polymers for the different battery components Progress in Energy and Combustion Science 79:100846 doi:10.1016/j.pecs.2020.100846
7. Deimede V, Elmasides C (2015) Separators for Lithium-Ion Batteries: A Review on the Production Processes and Recent Developments Energy Technology 3:453-468 doi:10.1002/ente.201402215
8. Du QC et al. (2019) Bendable Network Built with Ultralong Silica Nanowires as a Stable Separator for High-Safety and High-Power Lithium-Metal Batteries ACS applied materials & interfaces 11:34895-34903 doi:10.1021/acsami.9b09722
9. Feng X, Ren D, He X, Ouyang M (2020) Mitigating Thermal Runaway of Lithium-Ion Batteries Joule 4:1-28 doi:10.1016/j.joule.2020.02.010
10. Hao W, Kong D, Xie J, Chen Y, Ding J, Wang F, Xu T (2020) Self-Polymerized Dopamine Nanoparticles Modified Separators for Improving Electrochemical Performance and Enhancing Mechanical Strength of Lithium-Ion Batteries Polymers 12:648 doi:10.3390/polym12030648

11. Hu S et al. (2016) Novel aramid nanofiber-coated polypropylene separators for lithium ion batteries Journal of Materials Chemistry A 4:3513-3526 doi:10.1039/c5ta08694a
12. Huang C, Ji H, Guo B, Luo L, Xu W, Li J, Xu J (2019) Composite nanofiber membranes of bacterial cellulose/halloysite nanotubes as lithium ion battery separators Cellulose 26:6669-6681 doi:10.1007/s10570-019-02558-y
13. Huang Q, Zhao C, Li X (2021) Enhanced electrolyte retention capability of separator for lithium-ion battery constructed by decorating ZIF-67 on bacterial cellulose nanofiber Cellulose 28:3097-3112 doi:10.1007/s10570-021-03720-1
14. Jabbour L, Bongiovanni R, Chaussy D, Gerbaldi C, Beneventi D (2013) Cellulose-based Li-ion batteries: a review Cellulose 20:1523-1545 doi:10.1007/s10570-013-9973-8
15. Jana KK, Lue SJ, Huang A, Soesanto JF, Tung K-L (2018) Separator Membranes for High Energy-Density Batteries ChemBioEng Reviews 5:346-371 doi:10.1002/cben.201800014
16. Jia S, Yang S, Zhang M, Huang K, Long J, Xiao J (2020) Eco-friendly xonotlite nanowires/wood pulp fibers ceramic hybrid separators through a simple papermaking process for lithium ion battery Journal of Membrane Science 597:117725 doi:10.1016/j.memsci.2019.117725
17. Lee H, Yanilmaz M, Toprakci O, Fu K, Zhang X (2014) A review of recent developments in membrane separators for rechargeable lithium-ion batteries Energy Environ Sci 7:3857-3886 doi:10.1039/c4ee01432d
18. Li H, Wu D, Wu J, Dong LY, Zhu YJ, Hu X (2017) Flexible, High-Wettability and Fire-Resistant Separators Based on Hydroxyapatite Nanowires for Advanced Lithium-Ion Batteries Advanced Materials 29:1703548 doi:10.1002/adma.201703548
19. Liu J et al. (2021) A high-safety and multifunctional MOFs modified aramid nanofiber separator for lithium-sulfur batteries Chemical Engineering Journal 411:128540 doi:10.1016/j.cej.2021.128540
20. Liu J, Yang K, Mo Y, Wang S, Han D, Xiao M, Meng Y (2018) Highly safe lithium-ion batteries: High strength separator from polyformaldehyde/cellulose nanofibers blend Journal of Power Sources 400:502-510 doi:10.1016/j.jpowsour.2018.08.043
21. Liu L et al. (2020a) Comprehensively-upgraded polymer electrolytes by multifunctional aramid nanofibers for stable all-solid-state Li-ion batteries Nano Energy 69:104398 doi:10.1016/j.nanoen.2019.104398
22. Liu X, Zhang B, Wu Y, Chen J, Fang M, Wang L, Wang L (2020b) The effects of polybenzimidazole nanofiber separator on the safety and performance of lithium-ion batteries: Characterization and analysis from the perspective of mechanism Journal of Power Sources 475:228624 doi:10.1016/j.jpowsour.2020.228624
23. Luo J, Zhang M, Yang B, Liu G, Tan J, Nie J, Song S (2019) A promising transparent and UV-shielding composite film prepared by aramid nanofibers and nanofibrillated cellulose Carbohydr Polym 203:110-118 doi:10.1016/j.carbpol.2018.09.040
24. Lv D et al. (2021) Pure cellulose lithium-ion battery separator with tunable pore size and improved working stability by cellulose nanofibrils Carbohydr Polym 251:116975

doi:10.1016/j.carbpol.2020.116975

25. Manthiram A (2017) An Outlook on Lithium Ion Battery Technology ACS Central Science 3:1063-1069 doi:10.1021/acscentsci.7b00288
26. Mao Y et al. (2021) A high strength hybrid separator with fast ionic conductor for dendrite-free lithium metal batteries Chemical Engineering Journal 416:129119 doi:10.1016/j.cej.2021.129119
27. Nabipour H, Nie S, Wang X, Song L, Hu Y (2019) Highly flame retardant zeolitic imidazole framework-8@cellulose composite aerogels as absorption materials for organic pollutants Cellulose 27:2237-2251 doi:10.1007/s10570-019-02860-9
28. Pan R, Wang Z, Sun R, Lindh J, Edström K, Strømme M, Nyholm L (2017) Thickness difference induced pore structure variations in cellulosic separators for lithium-ion batteries Cellulose 24:2903-2911 doi:10.1007/s10570-017-1312-z
29. Patel A et al. (2020) High Modulus, Thermally Stable, and Self-Extinguishing Aramid Nanofiber Separators ACS applied materials & interfaces 12:25756-25766 doi:10.1021/acsami.0c03671
30. Sheng J, Chen T, Wang R, Zhang Z, Hua F, Yang R (2020) Ultra-light cellulose nanofibril membrane for lithium-ion batteries Journal of Membrane Science 595:117550 doi:10.1016/j.memsci.2019.117550
31. Sheng J, Tong S, He Z, Yang R (2017) Recent developments of cellulose materials for lithium-ion battery separators Cellulose 24:4103-4122 doi:10.1007/s10570-017-1421-8
32. Tan L et al. (2020) Preparation and Properties of an Alginate-Based Fiber Separator for Lithium-Ion Batteries ACS applied materials & interfaces 12:38175-38182 doi:10.1021/acsami.0c10630
33. Wang Z, Xiang H, Wang L, Xia R, Nie S, Chen C, Wang H (2018) A paper-supported inorganic composite separator for high-safety lithium-ion batteries Journal of Membrane Science 553:10-16 doi:10.1016/j.memsci.2018.02.040
34. Waqas M, Ali S, Feng C, Chen D, Han J, He W (2019) Recent Development in Separators for High-Temperature Lithium-Ion Batteries Small 15:1901689 doi:10.1002/smll.201901689
35. Wen H et al. (2017) Sustainable and Superior Heat-Resistant Alginate Nonwoven Separator of $LiNi_{0.5}Mn_{1.5}O_4$/Li Batteries Operated at 55 °C ACS applied materials & interfaces 9:3694-3701 doi:10.1021/acsami.6b14352
36. Wen L, Liang J, Chen J, Chu Z, Cheng H, Li F (2019) Smart Materials and Design toward Safe and Durable Lithium Ion Batteries Small Methods 3:1900323 doi:10.1002/smtd.201900323
37. Xu K, Qin Y, Xu T, Xie X, Deng J, Qi J, Huang C (2019) Combining polymeric membranes with inorganic woven fabric: Towards the continuous and affordable fabrication of a multifunctional separator for lithium-ion battery Journal of Membrane Science 592:117364 doi:10.1016/j.memsci.2019.117364
38. Xu Q, Wei C, Fan L, Peng S, Xu W, Xu J (2017) A bacterial cellulose/Al_2O_3 nanofibrous composite membrane for a lithium-ion battery separator Cellulose 24:1889-1899 doi:10.1007/s10570-017-1225-x

39. Yang B, Wang L, Zhang M, Luo J, Lu Z, Ding X (2020a) Fabrication, Applications, and Prospects of Aramid Nanofiber Advanced Functional Materials 30:2000186 doi:10.1002/adfm.202000186
40. Yang H, Shi X, Chu S, Shao Z, Wang Y (2021) Design of Block-Copolymer Nanoporous Membranes for Robust and Safer Lithium-Ion Battery Separators Advanced Science 8:2003096 doi:10.1002/advs.202003096
41. Yang M et al. (2011) Dispersions of Aramid Nanofibers: A New Nanoscale Building Block ACS Nano 5:6945–6954 doi:10.1021/nn2014003
42. Yang Y, Huang C, Gao G, Hu C, Luo L, Xu J (2020b) Aramid nanofiber/bacterial cellulose composite separators for lithium-ion batteries Carbohydr Polym 247:116702 doi:10.1016/j.carbpol.2020.116702
43. Zhai P, Liu K, Wang Z, Shi L, Yuan S (2021) Multifunctional separators for high-performance lithium ion batteries Journal of Power Sources 499:229973 doi:10.1016/j.jpowsour.2021.229973
44. Zhang F, Lan X, Peng H, Hu X, Zhao Q (2020) A “Trojan Horse” Camouflage Strategy for High-Performance Cellulose Paper and Separators Advanced Functional Materials 30:2002169 doi:10.1002/adfm.202002169
45. Zhang H, Wang X, Liang Y (2015) Preparation and characterization of a Lithium-ion battery separator from cellulose nanofibers Heliyon 1:e00032 doi:10.1016/j.heliyon.2015.e00032
46. Zhang J et al. (2014) Sustainable, heat-resistant and flame-retardant cellulose-based composite separator for high-performance lithium ion battery Scientific reports 4:3935 doi:10.1038/srep03935
47. Zhang L, Li X, Yang M, Chen W (2021a) High-safety separators for lithium-ion batteries and sodium-ion batteries: advances and perspective Energy Storage Materials 41:522–545 doi:10.1016/j.ensm.2021.06.033
48. Zhang TW, Tian T, Shen B, Song YH, Yao HB (2019) Recent advances on biopolymer fiber based membranes for lithium-ion battery separators Composites Communications 14:7-14 doi:10.1016/j.coco.2019.05.003
49. Zhang X et al. (2021b) Recent progress in flame-retardant separators for safe lithium-ion batteries Energy Storage Materials 37:628-647 doi:10.1016/j.ensm.2021.02.042
50. Zhu C et al. (2019) Aramid nanofibers/polyphenylene sulfide nonwoven composite separator fabricated through a facile papermaking method for lithium ion battery Journal of Membrane Science 588:117-169 doi:10.1016/j.memsci.2019.117169
51. Zhu C et al. (2020) Facile fabrication of cellulose/polyphenylene sulfide composite separator for lithium-ion batteries Carbohydr Polym 248:116753 doi:10.1016/j.carbpol.2020.116753

Figures

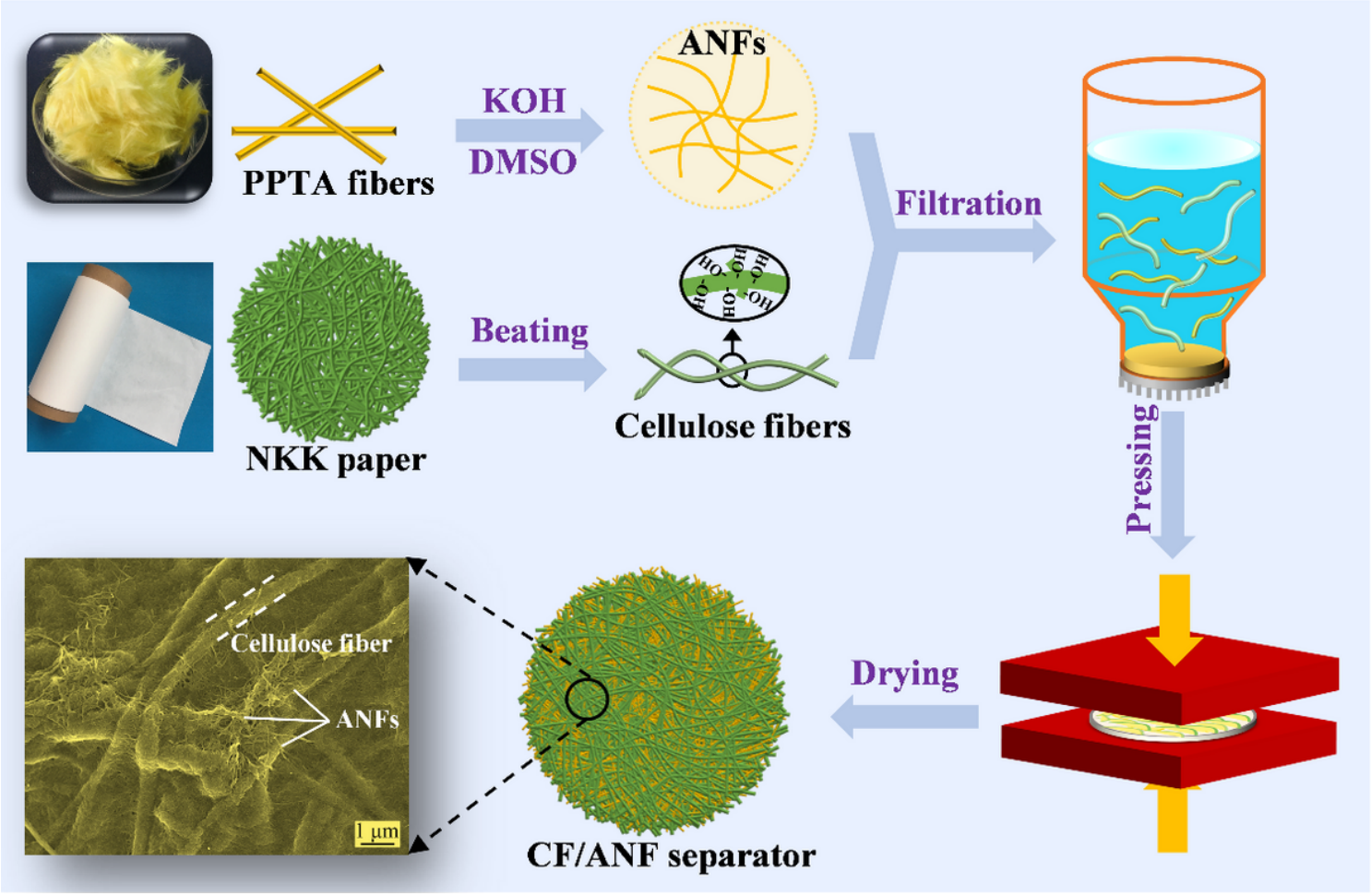

Figure 1

Schematic illustration for the preparation of CF/ANF composite separator.

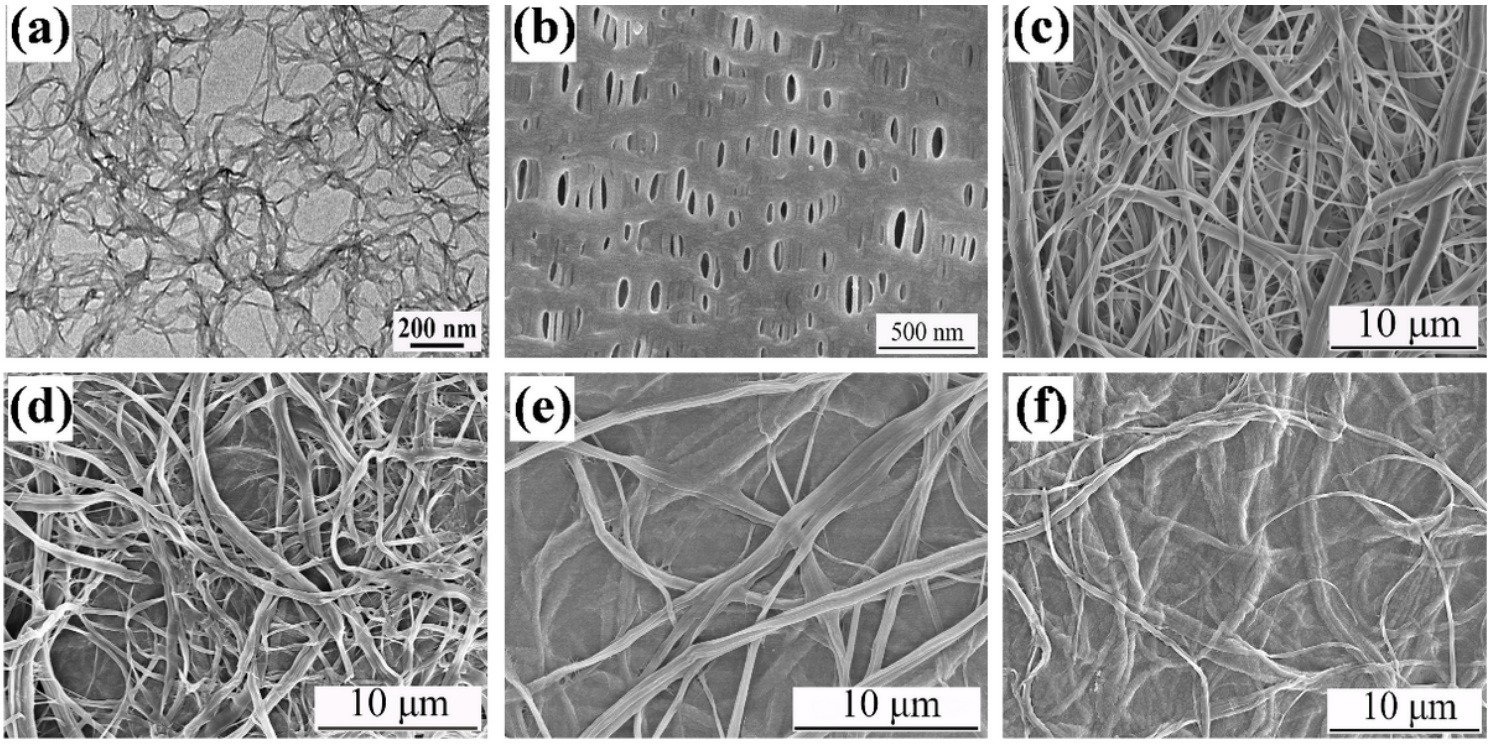

Figure 2

Morphologies of (a) ANFs; (b) PP membrane; (c) CF membrane; (d) CF/ANF-10 membrane; (e) CF/ANF-20 membrane and (f) CF/ANF-30 membrane.

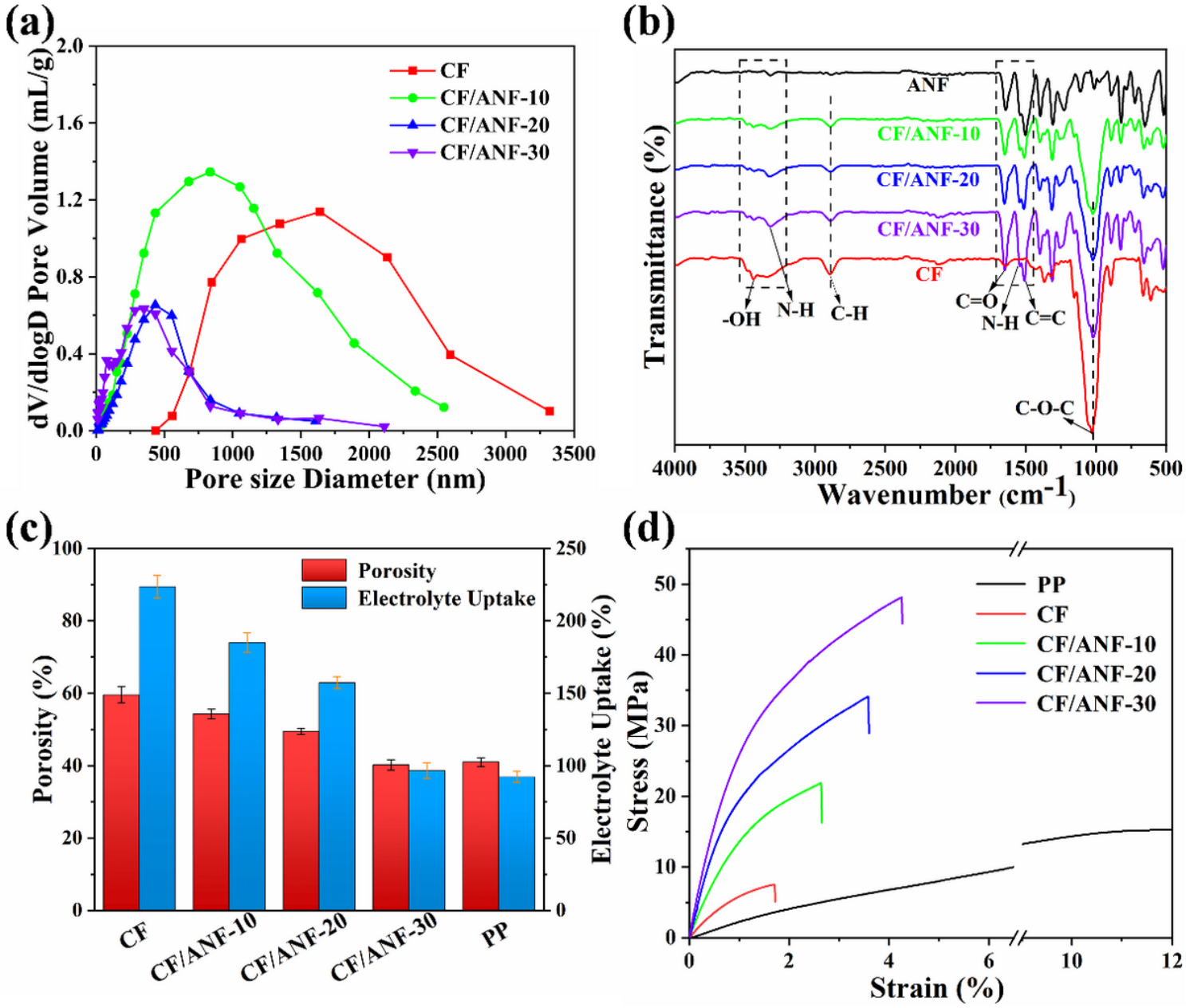

Figure 3

(a) Pore size distribution of CF and CF/ANF composite membranes; (b) FT-IR spectra of CF and CF/ANF composite membranes; (c) porosity and electrolyte uptake of PP, CF and CF/ANF composite membranes; (d) tensile strength of PP (transverse direction), CF and CF/ANF composite membranes.

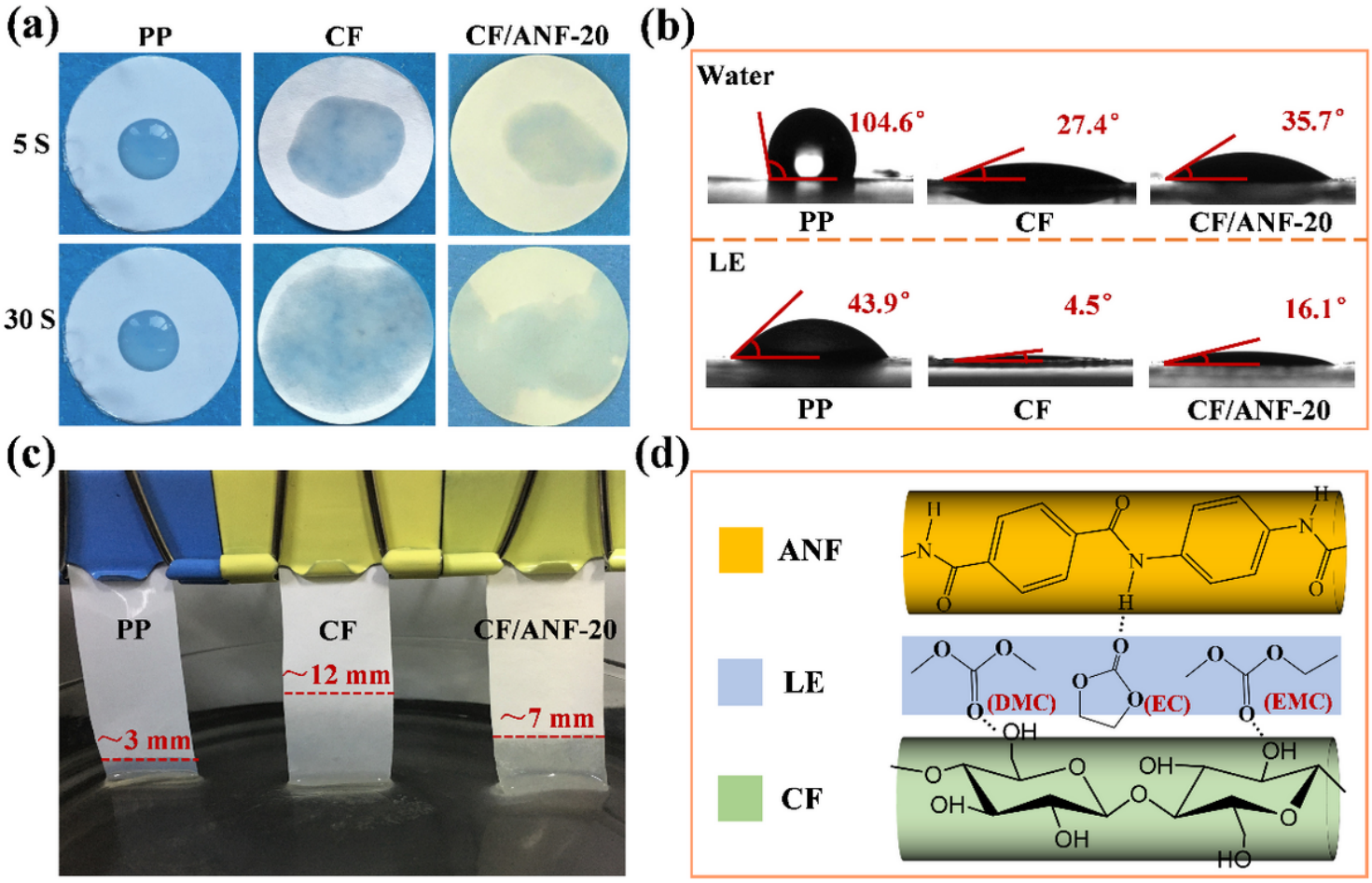

Figure 4

(a) Wettability images of PP, CF and CF/ANF-20 separators after 5 s and 30 s; (b) contact angle images of the separators; (c) electrolyte-immersion height of the separators; (d) schematic principle of the interaction between CF/ANF-20 separator and the liquid electrolyte.

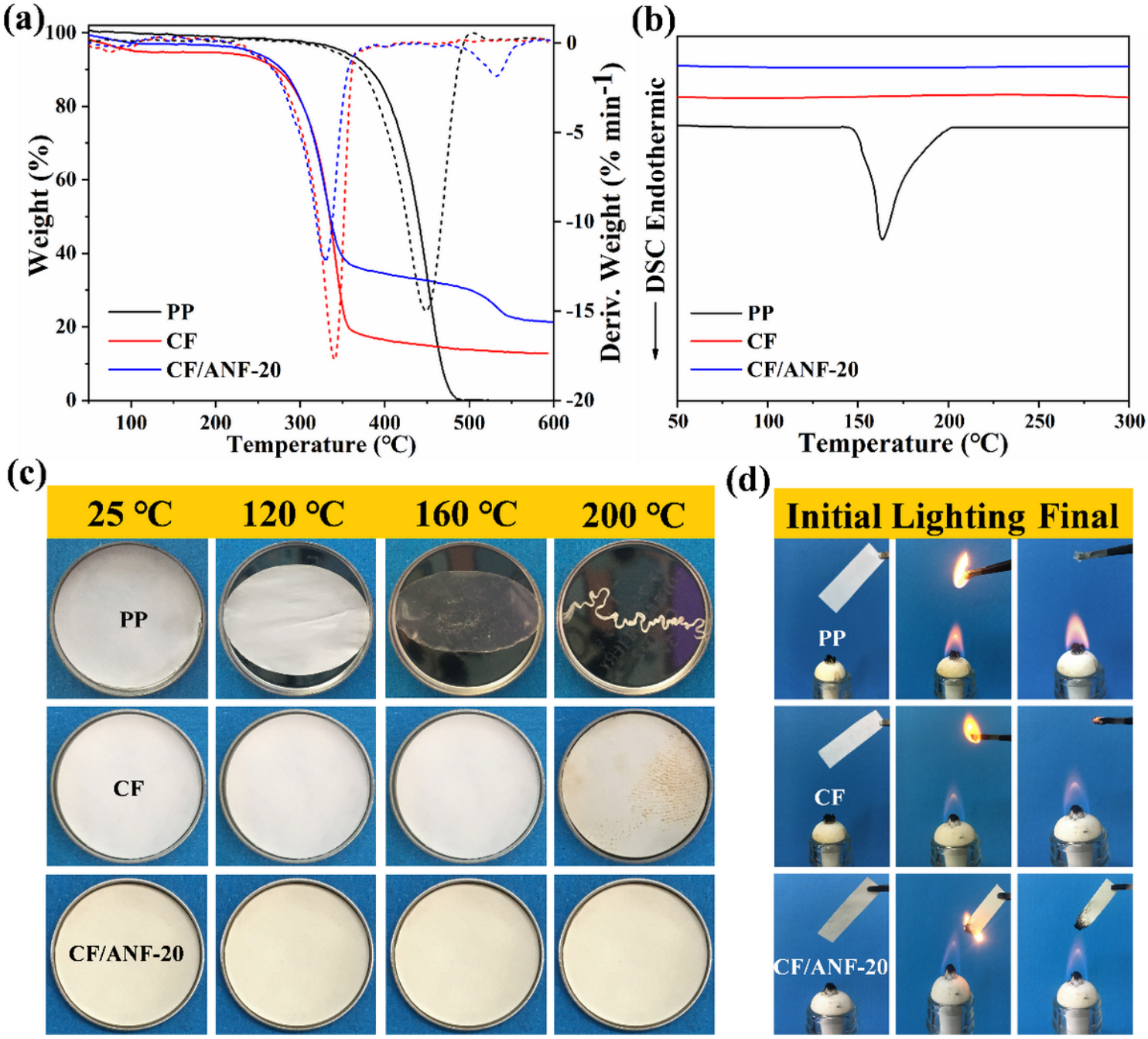

Figure 5

(a) TG–DTG curves and (b) DSC curves of PP, CF and CF/ANF-20 separators; (c) photographs of the separators before and after heat treatment at different temperatures for 0.5 h.; (d) combustion behavior of the separators.

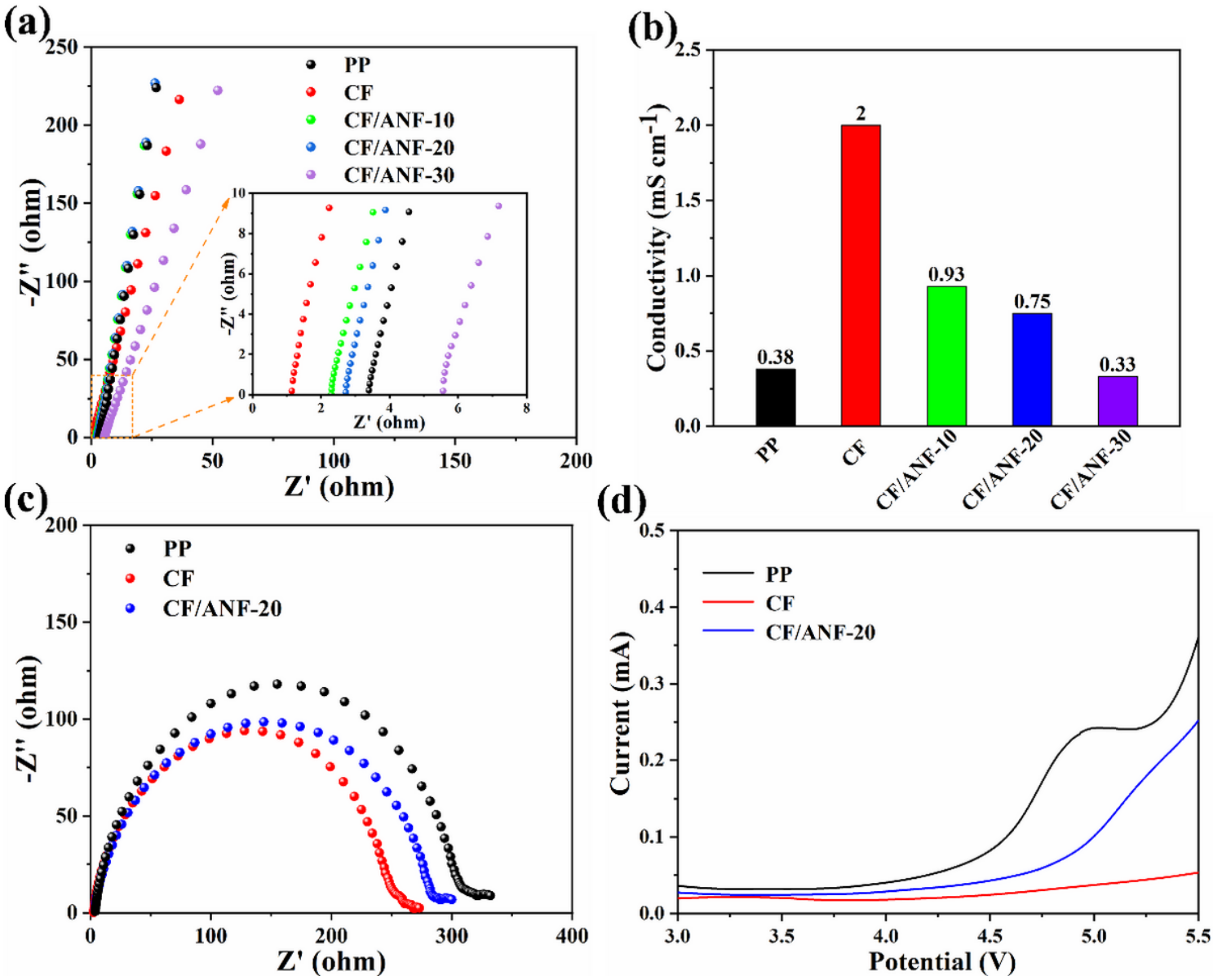

Figure 6

(a) EIS profiles of SS/separator/SS cells with PP, CF or CF/ANF composite membranes as the separator; (b) the corresponding ionic conductivity of the membranes; (c) Nyquist plots of Li/separator/Li cells based on PP, CF or CF/ANF-20 separator; (d) Linear sweep voltammetry curves of SS/separator/Li cells using PP, CF or CF/ANF-20 separator.

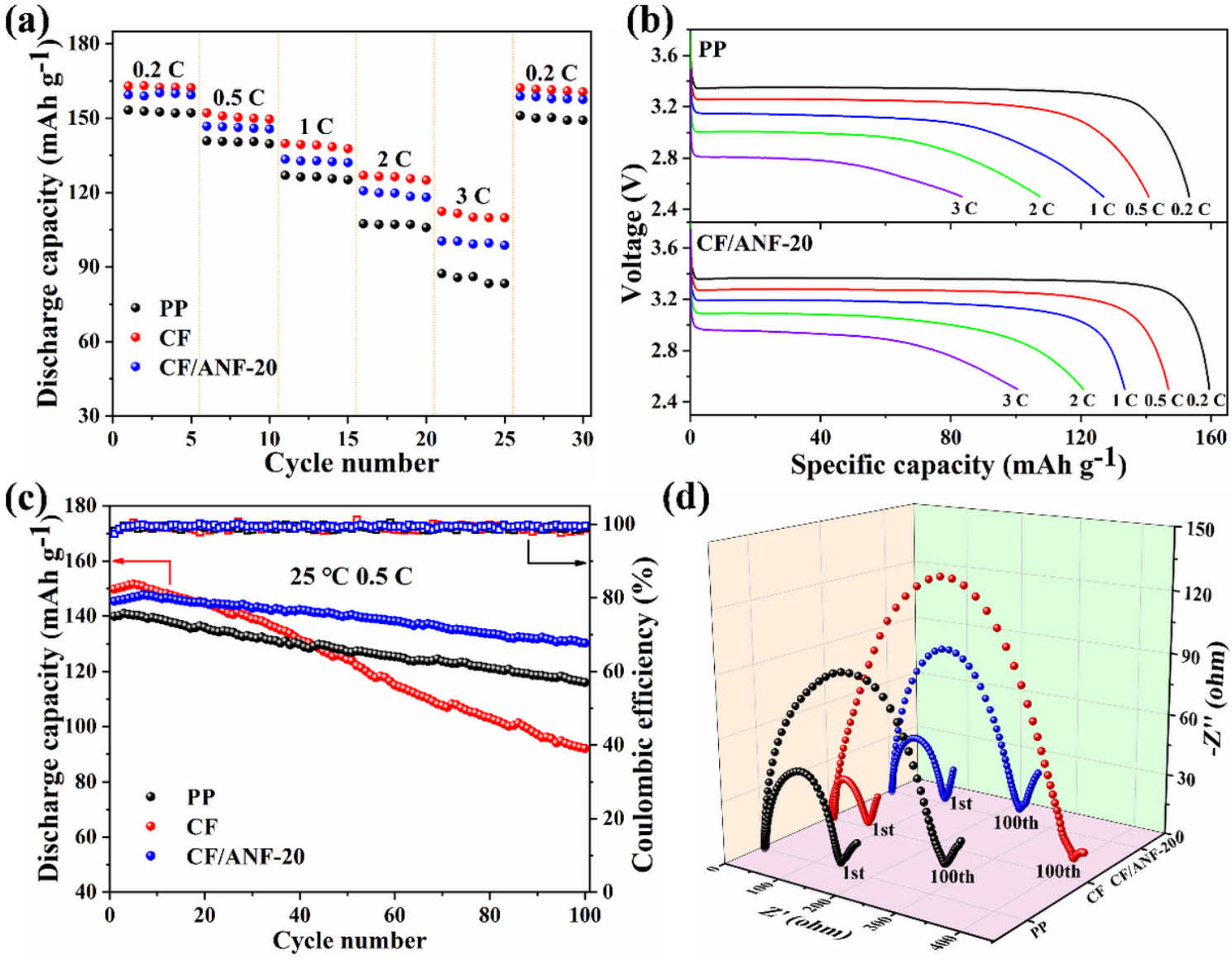

Figure 7

(a) Discharge rate capability of LiFePO4/Li cells with PP, CF and CF/ANF-20 separators at current density of 0.2 C to 3 C.; (b) discharge profiles of the cells using PP or CF/ANF-20 separators; (c) Cycling performance of the cells assembled with PP, CF and CF/ANF-20 separators at charge/discharge current density of 0.5 C/0.5 C; (d) Nyquist plots of the cells with PP, CF and CF/ANF-20 separators after the first cycle and the 100th cycle, respectively.

Supplementary Files

This is a list of supplementary files associated with this preprint. Click to download.

- Graphicalabstract.png
- SupportingInformation.docx